AD-A048 065 NAVAL POSTGRADUATE SCHOOL MONTEREY CALIF F/G 11/6
A STUDY OF THE EFFECT OF VELOCITY ON CORROSION OF GALVANIC COUP--ETC(U)
DEC 77 J PERKINS, K J GRAHAM, G STORM

UNCLASSIFIED NPS-69PS-77-004 NL

1 OF 1
AD A048 065

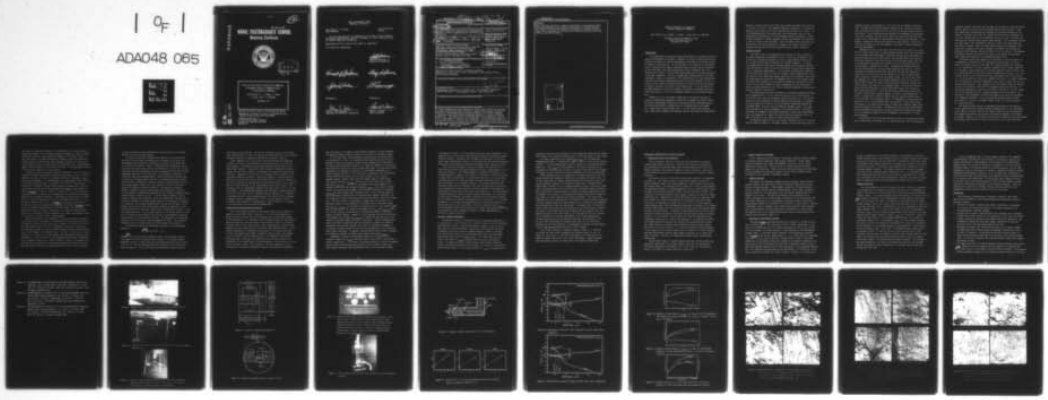

END
DATE FILMED
1-78
DDC

(12)

NPS-69PS-77-004

NAVAL POSTGRADUATE SCHOOL

Monterey, California

A STUDY OF THE EFFECT OF VELOCITY ON CORROSION OF GALVANIC COUPLES IN SEAWATER USING A CIRCLING-FOIL APPARATUS

Jeff Perkins, K. J. Graham, G. Storm,
J. Locke, and J. R. Cummings

December 1977

Technical Report No. 4
To the Office of Naval Research
Contract No. N00014-77-WR-70215
NR-036-120

NAVAL POSTGRADUATE SCHOOL
Monterey, California

Rear Admiral I. W. Linder
Superintendent

Jack R. Borsting
Provost

The work reported herein was supported by the Office of Naval Research, Metallurgy Program Office, Code 471, Arlington, VA 22217, through Contract No. N00014-77-WR-70215, NR-036-120.

This report was prepared by:

Jeff Perkins
Associate Professor of
Mechanical Engineering

K. J. Graham, Research Chemist, NPS

G. Storm, LT, USN

J. Locke, LT, USN

J. R. Cummings, LT, USN

Reviewed by:

Allen E. Fuhs, Chairman
Department of Mechanical Engineering

Released by:

Robert R. Fossum
Dean of Research

(9) Technical rept. no. 4, Mar – Nov 77,

UNCLASSIFIED

SECURITY CLASSIFICATION OF THIS PAGE (When Data Entered)

REPORT DOCUMENTATION PAGE

READ INSTRUCTIONS BEFORE COMPLETING FORM

(14) 1. REPORT NUMBER: NPS-69PS-77-004

2. GOVT ACCESSION NO.

3. RECIPIENT'S CATALOG NUMBER

(6) 4. TITLE (and Subtitle): A STUDY OF THE EFFECT OF VELOCITY ON CORROSION OF GALVANIC COUPLES IN SEAWATER USING A CIRCLING-FOIL APPARATUS.

5. TYPE OF REPORT & PERIOD COVERED: Interim, 3/77 to 11/77

6. PERFORMING ORG. REPORT NUMBER: Technical Report No. 4

(10) 7. AUTHOR(s): Jeff/Perkins, Kenneth J./Graham, Gr[illegible]ry/Storm, John/Locke[illegible]/[redacted] J. R./Cummings

8. CONTRACT OR GRANT NUMBER(s): ~~N00014-77-WR-70215~~, NR-036-120

9. PERFORMING ORGANIZATION NAME AND ADDRESS: Materials Science and Chemistry Group, Code 69Ps, Department of Mechanical Engineering, Naval Postgraduate School, Monterey, CA 93940

10. PROGRAM ELEMENT, PROJECT, TASK AREA & WORK UNIT NUMBERS: Program Element: 61153N; Project: RR022-08-01

11. CONTROLLING OFFICE NAME AND ADDRESS: Office of Naval Research, Metallurgy Program Office, Code 471, Arlington, VA 22217

(11) 12. REPORT DATE: Dec[redacted]77

13. NUMBER OF PAGES: ~~32~~ (12) 36p.

14. MONITORING AGENCY NAME & ADDRESS (if different from Controlling Office): (16) RR02208; (17) RR0220801

15. SECURITY CLASS. (of this report): Unclassified

15a. DECLASSIFICATION/DOWNGRADING SCHEDULE

16. DISTRIBUTION STATEMENT (of this Report)

Approved for public release; distribution unlimited.
Reproduction in whole or in part is permitted for any purpose of the United States Government.

17. DISTRIBUTION STATEMENT (of the abstract entered in Block 20, if different from Report)

18. SUPPLEMENTARY NOTES

Prepared for presentation at the NACE Unit T-7C Committee Symposium on "Marine Corrosion" at Corrosion/78, Houston, Texas, March 1978.

19. KEY WORDS (Continue on reverse side if necessary and identify by block number)

20. ABSTRACT (Continue on reverse side if necessary and identify by block number)

A unique apparatus has been developed to study velocity effects on corrosion processes, and has been used initially to expose single metals and galvanic couples of some common marine structural materials in synthetic seawater electrolyte, under controlled hydrodynamic conditions at various relative velocities. The sample-holder in the apparatus has a standard foil profile, with a turbulence trip wire at the leading edge. Direct determinations of turbulence intensity, boundary layer thickness, and surface shear stress were

DD FORM 1 JAN 73 1473 EDITION OF 1 NOV 65 IS OBSOLETE S/N 0102-014-6601 |

UNCLASSIFIED

SECURITY CLASSIFICATION OF THIS PAGE (When Data Entered)

251450

Block 20

made at various velocities, enabling correlations of hydrodynamic models with electrochemical data and other observations of corrosion behavior. The effects of velocity and potential distribution on average corrosion rates, and on the mode and distribution of corrosive attack and corrosion products, have been studied.

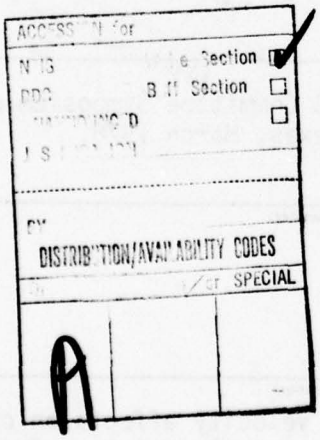

EFFECT OF VELOCITY ON CORROSION OF GALVANIC COUPLES IN SEAWATER

Jeff Perkins, K.J. Graham, G. Storm, J. Locke, and J.R. Cummings

Materials Science and Chemistry Group
Naval Postgraduate School
Monterey, CA 93940

INTRODUCTION

It is well-known that relative electrolyte velocity can strongly influence rates and mechanisms of corrosion. However, the study of velocity effects on corrosion is subject to conflicting demands, as pointed out in recent reviews by Syrett (1) and Davis (2). On the one hand, it is difficult in laboratory tests to duplicate the complex conditions found in actual service situations. On the other hand, tests which approximate service conditions tend to be imprecise with respect to control and characterization of the rate and nature of the flow conditions. This is a dilemma which obviously must be met with compromise. However, historically, flow characteristics of test systems have typically not been well-characterized, and in the data available in the literature (3-10), there is limited correlation of results from one test method to another, and much of the data is only qualitative. As is pointed out in the NACE Standard on laboratory testing, the ability to correlate data with other test results is one of the desirable features of any corrosion experiment.

Therefore, one of the primary objectives of the present work was to develop an experimental apparatus in which it is possible to closely control and monitor hydrodynamic conditions in situations which reasonably approximate those encountered by common alloys in a dynamic marine environment (e.g. ships hulls, piping systems, etc.). In the initial work reported here, single metal exposures and galvanic couples involving 70/30 cupronickel,

K-Monel, and plain carbon steel (PCS) were studied at modest flow rates (up to 3 m/sec, 10 ft/sec). The apparatus employed consisted of a cylindrical exposure tank, within which a foil specimen-carrier moved in a circle. The flow characteristics of the system were first established, and the static polarization characteristics of the independent metals determined. During dynamic exposures of couples, galvanic current was monitored as a function of time at various test velocities. Also, corrosion product morphology and distribution, and the distribution of damage on the sample surfaces was studied, macroscopically and microscopically, after various exposures.

APPARATUS DESIGN

An overall view of the apparatus which evolved is shown in Figure 1. The tank, constructed of plexiglass is 91.44 cm (36 in) in diameter, 45.75 cm (18 in) in height and filled to a level of approximately 30.48 cm (12 in) to hold 189.27 liters (50 gallons) of synthetic seawater. A system of plexiglass baffle strips was installed symmetrically along the interior sides and bottom in order to keep the electrolyte from stirring during high velocity experiment measurements. In the initial configuration, stirring did not occur until about 120 rpm (3.27 m/sec); simple modifications to the tank and foil will enable much higher velocities to be studied in the future. The tank bottom was fitted with an embedded 60.96 cm (24 in) diameter aeration canal which allowed air to be bubbled through the electrolyte from an array of 12 air holes spaced 30° apart; compressed air was provided by a bottle of carbon dioxide free air with an attached regulator to provide for precise control of the aeration.

The rotating foil assembly consisted of a plexiglass specimen-carrying foil suspended 10.16 cm (4 in) below the surface of the electrolyte by a 21.59 cm (8.5 in) vertical plexiglass support arm (Figure 2). The vertical support arm was streamlined to reduce drag and keep stirring to a minimum, and was attached to a 50.80 cm (20 in) horizontal plexiglass support arm suspended below a 3.175 cm (1.25 in) diameter plexiglass shaft. The shaft was connected via a pulley arrangement to an electric motor. The entire rotating foil assembly was statically balanced to reduce shaft and bearing wear, and supported by a large cross-piece that was connected to the top edge of the tank at four places to insure lateral stability.

The metallic sample couples were located topside in the foil, in round holes as shown in Figure 3. Proximate couples, in which the metals were in

physical contact, were placed in a 3.175 cm (1.25 in) diameter centerline hole. Couples that were electrically coupled but not in physical contact with one another were placed in 1.90 cm (0.75 in) diameter inboard and outboard holes. The specimen holes were machined to accommodate the specimens with close tolerance, so that once in place they were flush with the foil surface, and a watertight fit was obtained; by mounting the specimens in this manner, a minimum of solution disturbance was also realized. Figure 4 represents the details of the foil geometry, and Figure 5 shows the specimen mounting arrangement.

Specimens were set in the top of the foil and held in place by a tight press fit and a thin layer of liquid paraffin applied around the circumference of the specimen before placement. Electrical contact was accomplished via platinum discs fitted into the bottom of the specimen holes; the platinum discs were soldered to electrical leads of low resistance copper wire, and as the specimen was pressed into the hole, it was forced down upon the platinum disc to complete the circuit. Specimens were removed from the foil by pushing them out from the bottom, through an access hole. When a specimen or specimens were mounted, and before the foil was immersed in electrolyte, the access hole in the bottom of the foil was sealed watertight by means of a nylon screw and rubber o-ring. The electrical circuit was completed by a sealed wire running through the foil, up the vertical support arm, through the center of the horizontal plexiglass support arm and up through the center of the plexiglass shaft. The foil and vertical support arm were detachable from the horizontal support arm by way of a BNC electrical connector. All joints and access points were sealed with Silaster 732 RTV general purpose sealant to insure a watertight route. In order to transmit the electrical signal from the internal system circuit to the external current-sensing circuit, an arrangement of brass rings and brushes on top of the plexiglass shaft was employed. Brass brushes were positioned to rest against brass rings, to which were soldered copper wires from the interior of the shaft. The galvanic current between electrically coupled specimens when moving at various velocities was monitored by means of a zero-resistance ammeter circuit arrangement, with output to a strip chart recorder.

In addition to the brass ring contacts, the top of the shaft was fitted with a pulley wheel, providing a 5 to 1 speed reduction, and a 60-tooth gear.

A magnetic pickup, positioned near the gear and attached to a digital counter, sensed a magnetic flux as each tooth passed during shaft rotation. These flux signals were instantaneously converted into rpm and displayed by the counter. The shaft was driven via a pulley and V-belt drive arrangement by a 1/15 HP variable rpm D.C. motor capable of up to 1725 rpm. The motor was controlled by a Minarik Speed Control model SH-63AH. This arrangement allowed the shaft speed to be controlled to within ± 1 rpm at all times under any condition of loading. Where the shaft passed through the plexiglass cross-piece, which supported the entire assembly, two sealed, self-lubricating precision roller bearings coupled the shaft to the cross-piece. The bearings allowed for low-friction motion of the shaft at all speeds and prevented shaft wobble and vibration to the maximum possible extent.

The present method and apparatus for the study of velocity effects can be regarded as a variation on the rotating disc-plate method, in which a sample is deployed near the outer edge of a large non-conducting, rotating, circular disc-plate. The foil, however, represents only a small element of the disc-plate, thus giving rise to much less drag for a given velocity, and much higher velocities are possible without significant stirring. Also, centrifugal forces on the fluid are much less, and radial flow of electrolyte, such as occurs over the surface of a complete disc-plate, is largely eliminated. Flow is more nearly perfectly tangential to the circle of revolution of the specimen-carrying foil. Also, design of the foil profile allows for precise control of the nature of flow over the specimen location in the foil. In the present experiments, a platinum trip wire on the nose of the foil caused flow to be turbulent over the specimen locations at most velocities. An extension of the experiments reported here might be to cause the transition from laminar-to-turbulent flow to occur <u>on</u> the specimen surface (rather than before it, as here), allowing a direct study of the surface effects for a given velocity.

The present scheme retains one potential deficiency of any rotating method, namely that the specimen follows a repeated path in the electrolyte that brings it in effect into its own "wake", with the ionic contributions and dynamic disturbances introduced by the previous passages of the specimen holder. However, in the present case, the foil design was such that dynamic disturbances were minimal; the motion of the foil in the tank caused very

little wake effect, consisting only of a dispersion of small entrained bubbles which rapidly dispersed. Therefore, the present apparatus comprises a compact and efficient means of deploying specimens under quite well-characterized hydrodynamic conditions. Probably the only superior method would be a well-designed and characterized flow channel. However, the rotating foil tank involves much less space and electrolyte volume than would be required for a flow channel with similar velocity capability and flow characteristics. As noted earlier, there are always some compromises to be met in laboratory experimentation.

PROCEDURE FOR EXPOSURE OF SPECIMENS

The metals studied initially included 70/30 cupronickel (MILSPEC MIL-C-15726E), K-Monel (MIL-SPEC QQ-N-286 Class A), and a low carbon steel (AISI 1015). Specimens were cut to 1cm x 1cm x 0.75cm (0.394in. x 0.394in. x 0.295 in.) coupons, milled on all surfaces. Prior to mounting, the surface of each specimen underwent a standard preparation sequence, so as to minimize the effects of variations in surface roughness and cleanliness. Specimens were exposed physically coupled, electrically coupled, and singly, each in its own mount type and size. All mounting was done in a cold-type quickmount for ease in grinding, polishing and deployment in the specimen-carrying foil.

For specimens physically separated but electrically coupled during exposure, mounts 1.91cm (0.75in.) in diameter were used, placed in the inboard and outboard specimen holes in the foil (Figure 4). After mounting, the specimens were ground to a thickness of exactly 0.75cm (0.295in.), finishing with 180-grit paper. The mounted specimens were then ultrasonically cleaned in distilled water for 5 minutes, rinsed in a mixture of alcohol and water, and dried. Specimens exposed singly were mounted, ground and cleaned exactly as stated above except that 3.18cm (1.25in.) diameter mounts were used, placed in the centerline specimen hole on the foil (Figure 4). For specimens to be physically coupled during exposure, mounting was done in specially designed aluminum mounting rings 3.18cm (1.25in.) in diameter (Figure 6). Small holes 0.476cm (0.1875in.) in diameter were drilled and tapped on opposite sides of the mounting and rings, screws placed in these holes were used to apply 0.7 N·cm (2 in-oz) of torque to the screws in each case, thus creating a reproducible interfacial contact stress for all couples. After mounting, the screws were removed and the remaining holes filled with paraffin. After grinding, polishing, and cleaning, all mounted specimens were kept in a vacuum chamber until exposed.

Before, during and after each exposure in the tank, the conductivity, temperature, and pH were checked. Conductivity was maintained between 22 and 24Ω·cm, pH between 8.0 and 8.4, and the temperature was 20°C± 1°C. The length of runs included about a 45 second immersion period prior to attainment of full velocity, and a 30 second removal time. As soon as the foil assembly was removed from the exposure tank, the surface of each specimen was gently rinsed with distilled water. In the case of static exposures of PCS, this invariably led to the removal or displacement of some loosely adherent corrosion product. Therefore a procedure of drying followed by a gentle rinse was preferable. For dynamic exposures at 1.5 m/sec (5 ft/sec) and above, the corrosion product on the surface was generally adherent to the metal surface, as it would have to be in order to maintain in the dynamic conditions, so that rinsing did not tend to damage or disturb the product. After rinsing, specimens were removed from their mounting holes in the foil and allowed to air dry. This procedure avoids damage to the surface structures while removing the electrolytic environment, but of course does not take into account differences, if any, between the wet and dry states of the corrosion products. This study examined only corrosion products after drying. Dried specimens were mounted on SEM stubs, and corrosion products and the attached metal surfaces (after corrosion product removal by ultrasonic cleaning) were examined at various useful magnifications. In this way, the physical effects of velocity on corrosion product morphology and base metal surface damage were studied.

Direct weight loss measurements were made after demounting the specimens, but the data obtained had significant scatter due to difficulties with the specimen demounting technique employed, and therefore the data is not reported here. In general this data corresponded with the weight loss expected from the galvanic current vs. time data, and indicated that there was little erosive (mechanical) component in the total weight loss for the velocities and times studied here. Approximately 50 runs of up to 24 hours were made in this initial phase of work; nearly all the exposures involved the three single metals mentioned (70-30 Cu-Ni, K-Monel, and PCS) and two couple types (70-30 Cu-Ni/PCS and K-Monel/PCS), with relative velocities up to about 3m/sec (10 ft/sec).

DYNAMIC FLOW CHARACTERIZATION

At fairly low relative velocities between metal and electrolyte, flow is laminar. Above a critical velocity flow becomes turbulent; a small element of fluid chosen at random may be moving in any direction, although averaged over the entire cross-section, the net movement is in the macroscopically apparent direction. The transition from one type of flow to the other does not occur at any precisely definable velocity, but over a range of velocities. The actual flow is dependent on such factors as surface roughness and mechanical vibrations, and is also a function of the geometry of the system. In order to differentiate between the laminar and turbulent flow regimes, a dimensionless parameter called the Reynold's Number, Re, is used, defined as $Re = ux\rho/\mu = ux/\nu$, where u is the fluid velocity, x is a characteristic dimension in the direction of flow, ρ is the density of the fluid, μ is the dynamic viscosity, and μ is the kinematic viscosity. In this study, the critical Reynold's Number corresponding to a flat plate approximation in a uniform flow field was used. In this case, the critical Reynold's Number at which the transition from lamellar to turbulent flow is assumed to be about $Re = 5 \times 10^5$.

Whatever the type of flow, there will be a laminar layer in immediate contact with the metal. Even when the flow is turbulent there will still be a thin laminar sublayer caused by viscous drag on the water by the metal surface. Within this laminar sublayer is a diffusional (or mass transfer) boundary layer, in which the relative velocity is small or nearly zero, and the rate controlling process is ionic diffusion. Outside this layer increased velocity causes convective diffusion to be the predominate mode of mass transport. The thickness of the diffusional (mass-transport) boundary layer, δ_d, is approximately related to that of the hydrodynamic boundary layer, δ_h, with a constant relative thickness given by $\delta_h/\delta_d \simeq S_c^{1/3}$, where S_c is the dimensionless Schmidt number, defined as $S_c = \nu/D = \mu\rho/D$; D is the diffusion coefficient of the reacting species. The larger the value of the Schmidt number, the thinner the diffusional layer and the more rapidly it develops (1). The thickness, δ_d, is generally less than about 10 μm for turbulent flow conditions, where the thickness of the hydrodynamic boundary layer is given by $\delta_h = 0.38 \times Re^{0.2}$, with x the distance from the leading edge of a flat plate. Thus the rate of mass transfer across the diffusional boundary layer tends to be inversely related to the thickness of the hydrodynamic boundary layer.

Due to the velocity gradient which exists across these boundary layers, a shear stress, τ_s, is established on the surface, which may be calculated from the hydrodynamic parameters already discussed, for a given geometry. The stresses calculated for average flow rates up to 100 ft/sec are quite low, always less than 1 PSI. However, as pointed out by Syrett (1), the shear stress is a direct measure of the thickness of the hydrodynamic boundary layer, and since τ_s can be directly measured (or calculated) for a given experimental arrangement, it is a characteristic flow parameter which could be used in reporting corrosion rates, e.g. mpy vs. τ_s. In the present experiments, τ_s was not directly measured, but was calculated, for the simple geometry of the system. τ_s is calculated to be approximately 0.0015 PSI for the test velocity of 5 ft/sec (1.5 m/sec) and 0.007 PSI for 10 ft/sec (3.0 m/sec).

The macroscopic geometry presented by the metal specimen or moving form to the fluid will greatly affect the resulting flow characteristics. A wedge-shaped body, for example, will cause a transition from the laminar to the turbulent flow regime at a much lower velocity or Reynold's Number than a streamlined foil. Also, the wake effects are quite different for different shaped forms. The foil profile used in the present experiments was used primarily to reduce wake effects to a minimum, and a trip wire on the nose was used to ensure turbulent flow over the entire top surface at all velocities. This arrangement leads to a quite simple flow situation, with symmetric geometry, no sharp changes in cross-section, no obstacles to flow, and no crevices or protusions. The present apparatus, for example, does not produce cavitation, which a good feature unless you want to study cavitation effects. Also, the flow is always "fully developed" with no "mixed-up flow" or other complexities.

Microscopic surface roughness is also a very important factor in characterizing the flow regime. Any local projections or depressions, including those due to buildup of corrosion products, and dissolution pitting, must be considered. If the flow is laminar and the height of the projection is small in comparison with the thickness of the diffusion boundary layer, then the flow over the surface will be virtually unaffected. If, on the other hand, the flow velocity is greater than some critical value the projection will cause localized turbulence on the downstream surface of the body. In the present studies, the effective surface "finish" of the anode is changing

with time, an unavoidable feature of the dissolution and corrosion product formation processes. For the times studied, the changes in surface topology experienced would not cause substantial changes in the nature of flow. In the early stages, the surface features lie entirely within the diffusional boundary layer; at longer times, when irregular formations of surface corrosion products begin to extend beyond the diffusional layer, the morphology begins to be affected by the flow, and vice versa. The morphological effects of flow will be reported in a later section.

Before the present corrosion tests were conducted, it was of interest to determine the flow characteristics within the test system. First, it was of interest to measure the level of turbulence (turbulence intensity) around the foil and specimens. If we define $\bar{V}$ as the time averaged (foil) velocity in the free stream direction, $\bar{V} = \frac{1}{t}\int_{o}^{t+t_o} V dt$, and V' is the velocity fluctuation of elements of fluid in the turbulent boundary layer, then the instantaneous velocity in the free stream direction of a given element of fluid is the sum of $\bar{V}$ and V', and $\overline{V'} = 0$. However, $\overline{V'^2}$ is non-zero, and the quantity $\sqrt{\overline{V'^2}}/\bar{V}$ is a measure of the magnitude of the turbulent disturbance, known as the "turbulence intensity". This quantity, which reflects the RMS value of velocity fluctuations in the flow, typically has values of 1 to 10 percent in turbulent tube flow. Typically, the velocity fluctuations in the flow (x) direction represented by $\sqrt{\overline{V_x'^2}}/\bar{V}_x$, are greater than in the transverse (y) direction (perpendicular to the foil surface here), $\sqrt{\overline{V_y'^2}}/\bar{V}_y$, particularly near the surface. Typically, the turbulence intensity rises from zero at the surface (laminar sublayer), to a peak, then gradually falls off (to zero if the bulk volume is large enough).

The flow was known to be turbulent at all test velocities by reason of foil design and the placement of a platinum trip wire 0.0508 cm (0.020 in.) in diameter on the upper foil surface at a distance of 0.3175 cm (0.125 in.) from the leading edge of the foil. Knowledge of the level of turbulence was important in order to properly evaluate surface corrosion product morphology, surface damage, and corrosion rates. The rate of corrosion, as stated earlier, is a function of the mass-transfer and hydrodynamic boundary layer thicknesses. It was crucial that these parameters be accurately determined for the dynamic system in use. Also, in spite of efforts to streamline the foil and vertical support arm, some solution disturbance (wake) was inevitable and certain flow patterns developed within the tank; it was necessary

to know the extent of these disturbances and their effect on the actual velocity over the specimens surface.

In order to accurately determine the character of the flow around the foil a hot-film probe was mounted over the upper foil surface, and measurements were obtained as a function of position on the surface and as a function of velocity. Figure 7 illustrates the configuration for a run with the hot-film probe over the centerline hole in the foil. The hot-film probe (hot-wire anemometer) was used to measure the flow velocity and turbulence intensity in the flow field. The principle of operation is relatively simple and straightforward. When an electrically heated wire is placed in a flowing stream, heat will be transferred between the wire and the stream, depending on a number of factors, including the flow rate. The sensing element consists of a short length of fine wire stretched between two supports as shown in Figure 8. One measuring technique employs a constant current passing through the sensing wire; variation in flow results in changed wire temperature, hence changed resistance, which thereby becomes a measure of flow. A second technique employs a servo-system to maintain wire resistance, hence wire temperature; and when the hot wire is placed in a flowing stream, heat will be transferred, primarily by convection. The sensing equipment used with the hot-film probe in the present case was a TSI model 1050 constant temperature anemometer, a TSI model 1051-1D monitor and power supply, and a TSI model RMS voltmeter. With the instrumented foil, runs were made starting at 20 rpm and going in steps up to 120 rpm (at speeds greater than 120 rpm, the measurements indicated that stirring in the tank became a factor). At each speed, the system was allowed to run for 30 minutes before readings were taken. The parameters monitored were D.C. bridge voltage (e), RMS voltage (e') and rpm (ω).

The governing relation for turbulence intensity in this measurement method is

$$\sqrt{\overline{V'^2}}/\bar{V} = 4e'V/(V^2 - V_o^2)$$

where $\sqrt{\overline{V'^2}}/\bar{V}$ is the turbulence intensity, and V is the apparent velocity (the speed of the foil calculated from the RPM), e' is the RMS voltage measured on the D.C. bridge, and V_o is an extrapolated value from the plot of e^2 vs. $\sqrt{V}$. The data obtained for several positions over the foil are shown in Figure 9. Once V_o was known the turbulence intensity could be

calculated for each position. For the two velocities used in the corrosion tests reported here, 5 ft/sec (55 rpm) and 10 ft/sec (100 rpm), the turbulence intensity levels at the specimen locations are tabulated in Table I.

After completion of a set of runs, the hot-film probe was raised 1mm (0.0394 in.) from its initial position on the surface of the foil and the runs repeated. The probe was then raised another millimeter and the procedure again repeated. This was done in an attempt to establish a velocity profile over the foil as well as to determine the turbulence intensity with certainty. Comparison of these sets of runs showed little variance in the calculated turbulence intensity. Because the design of the hot-film probe allowed it to be placed no closer than 2.03mm (0.08 in.) from the surface of the foil and because the sensing area of the probe was about one mil, measurement of the same velocity at all three heights above the foil lead to the conclusion that the hydrodynamic boundary layer was 2.0mm (0.079 in.) or less in thickness. The hydrodynamic boundary layer thickness, assuming turbulent flow over a flat plate, can be calculated from the equation $\delta_h = 0.38x/Re^{0.2}$, as mentioned earlier; using the parameters of the present foil and assuming a Reynold's Number of approximately 5×10^5, the above equation predicts a boundary layer thickness of approximately 1.75mm (0.0689 in.), in support of the conclusions from the film probe measurements.

POLARIZATION AND DEPOLARIZATION BEHAVIOR

One of the primary interests of the present study was the behavior of galvanic couples under dynamic conditions. It is of course incorrect to assume that the corrosion rate for a galvanic couple is determined simply by the difference in the potentials of the dissimilar metals on open circuit. When the metals are short-circuited, as when bolted, riveted, or otherwise connected electrically, other factors, such as polarization, relative areas, geometry, and the conductivity of the solution play important roles. In the present experiments, the exposed surface areas of the coupled metals were the same, the geometry was simple (co-planar, adjacent areas, with minimal crevice situation), and the conductivity of the (seawater) solution was relatively high. There were no variations in these factors which can be considered to have significantly affected changes in corrosion rate as a function of velocity or time. Also, because of the high conductivity of the electrolyte, no potential distribution effects were expected (or observed)

over the surface of the small, closely-placed specimens, and both proximate and separated couples showed the same sort of attack on the anodic member.

On the other hand, the polarization characteristics of various metals are distinctive, so that it is considered that observed velocity effects on galvanic currents and corrosive attack are most appropriately interpreted in terms of the polarization curves of the respective members of the couples. The polarization curves for the two couple types tested, obtained under static conditions, for specimens in mounted as in the dynamic deployments, are shown in Figures 10 and 11. It is seen that, as expected, both couple types (70/30 Cu-Ni:PCS and K-Monel:PCS) are under cathodic control (with a somewhat greater cathodic Tafel slope for K-Monel than for 70/30 Cu-Ni). Thus the net potential, E_{couple}, is very close to the open circuit anode potential, $E_{corr\ PCS}$. From this it is obvious that small changes in the cathodic Tafel slope will strongly influence i_{couple}, with cathodic depolarization, as expected under dynamic flow conditions, resulting in increased i_{couple} and thus a higher anodic corrosion rate. In this initial phase of work, polarization behavior was not monitored under dynamic conditions, but the single metal static polarization curves can be used as a basis for discussion. The first effect, as discussed, is simply that of coupling of the dissimilar metals, which increases the corrosion rate of the anodic member from i_{corr} to i_{couple}, and decreases the corrosion rate of the cathodic member. With the introduction of a dynamic environment, the i_{corr} and i_{couple} values will further increase, primarily due to increased provision of dissolved oxygen to cathodic regions. Oxygen is a very energetic cathodic de-polarizer, thus leading to an increase in i_{couple} for couples and thus the rate of corrosion of the anodic member (PCS in all cases here). Another de-polarizing effect that might be expected would be the removal of metal ions formed by dissolution at the anodic surface; this effect is considered secondary in the present situation because of the very low polarization of the anode even under static conditions. In general, de-polarization effects tend to decrease the respective cathodic and anodic Tafel slopes and increase i_{couple}.

Depending on whether de-polarization effects are strongest at the cathode or anode, the E_{couple} value will shift to more noble or more active values, respectively. In the case of the present couples, it would be expected that the major de-polarizing effects would be at the cathode, since even under static conditions the anode material (PCS) is not polarized strongly

(see Figures 10 and 11). At the velocities used in these experiments, it is expected that the rate controlling reaction is oxygen de-polarization under diffusion control. Therefore, from the shape and character of the single metal static polarization curves it is predicted that the corrosion reactions taking place under dynamic conditions are probably under diffusion control.

Also, the rate and manner in which the K-Monel and 70/30 Cu-Ni form their protective oxide films may determine the extent of polarization of the corrosion reactions. Even though oxygen is a cathodic de-polarizer, the increased supply of oxygen to the surface of the K-Monel or 70/30 Cu-Ni aids to some extent in maintenance of a protective oxide film, and a more noble corrosion potential for these materials, and this oxide film tends to promote polarization of the cathodic reaction. At increased velocities and relatively high levels of turbulence, the oxide film may tend to break down due to mechanical (erosive) effects, with the cupronickel film being more susceptible to these effects than that on the K-Monel (1). From the observed cathodic polarization curves of these respective materials, it is seen that the open circuit potential with PCS is greater for the cupronickel cathode, and the slope of the cathodic polarization curve is also less. If, as seems reasonable, it is assumed that depolarization of the K-Monel cathode is no greater than that of the cupronickel, it would be predicted that i_{couple} for cupronickel cathodes would continue to be higher under dynamic conditions. These predictions were confirmed by galvanic current measurements as a function of velocity and time.

GALVANIC CURRENT MEASUREMENTS

The galvanic current in separated electrical couples was monitored at 3 velocities, 0, 5 and 10 ft/sec (0, 1.5 and 3.0 m/sec), for 70/30 Cu-Ni/PCS and K-Monel/PCS couples. The data presented in Figures 12 and 13, and 14 shows that for static conditions, the galvanic current density decreased continuously with time, while the dynamic exposures exhibit an increase with time and with velocity; this correlates with visual and microscopic examinations which will be discussed later. All curves start (at time zero) at the value of i_{couple} predicted from the static polarization curves. The sharp increase in current density under dynamic conditions verifies the predicted behavior of the couples in relation to their polarization characteristics. The recorded increase in i_{couple} corresponds to an

increase in the rate of the reactions at the cathode and anode over the single metal values, and a greater corrosion rate of the anodic member of the couples.

The anodic corrosion rate is related to i_{couple} by the expression: CORROSION RATE (MPY) = $0.1288i(\mu A/cm^2)\ (\frac{eq\text{-}wt}{3\rho})$, where i is the current density ($\mu A/cm^2$), ρ is the specimen density (g/cm^3), and eq wt = specimen equivalent weight (g). The i_{couple} for PCS coupled to 70/30 Cu-Ni is greater at all velocities and increases with velocity at a greater rate than for PCS coupled to K-Monel, as seen in Figure 14, and as predicted in the earlier discussion.

Visual observations of the surfaces of the K-Monel and 70/30 Cu-Ni components provide some insight to differences in observed corrosion rates. At all test velocities the K-Monel surface exhibited the same dull luster which it had initially, typical of its protective oxide flim. Although nickel-copper alloys (K-Monel) do not in general exhibit as good as corrosion resistance as the cupro-nickel alloys (70/30 Cu-Ni) in stagnant seawater conditions [6], a particularly valuable feature of K-Monel and most nickel-based alloys in seawater is the ability of the protective surface oxide film to remain in good repair in highly turbulent and erosive conditions. This ability was evidenced here by the maintenance of the K-Monel film under dynamic conditions, the lower measured values of current density at all velocities, and somewhat less de-polarization than the cupro-nickel. The higher rate of de-polarization for the cupro-nickel, and the increase in the visible metallic luster of the surface of the cupro-nickel with increased velocity suggests that the protective surface oxide film formed on the 70/30 Cu-Ni may be more susceptible to breakdown in turbulent environments, effectively exposing more cathodic metal surface and increasing the galvanic current density (1,6). The very subtle differences in surface luster seen for the 70/30 Cu-Ni specimens did not lend themselves to photographic recording, and SEM observations at high magnifications also gave a little insight.

With further reference to regard to Figures 12 and 13, it should be noted that the time periods considered are extremely short; in fact in Figure 13, the current vs. time plot for K-Monel at 10 ft/sec has not yet reached a steady state value, and is still increasing. Longer exposures would obviously be useful to extend some of the ideas developed here.

MICROSCOPIC OBSERVATIONS OF VELOCITY EFFECTS

1. Single Metal and Static Exposures

Since the primary interest in this work was the behavior of galvanic couples under dynamic conditions, a baseline for microscopic observations was established by examining single metal coupons exposed under static and dynamic conditions, and galvanic couples for static exposures. These baseline observations were useful to interpret observations on couples in dynamic exposures.

The surface structure of PCS after single-metal exposures is represented in Figure 15. The structure after 24 hours static exposure consists of a loosely adherent (Figure 15a) bright orange rust, much of which tends to wash off during rinsing. The structure after 24 hours at 5 ft/sec is more adherent, macroscopically displays a streaked appearance, and is a darker orange; Figure 15b shows the structure observed via SEM. After 24 hours at 10 ft/sec, the structure is non-uniform and much more compact, (Figure 15c), and has a darker red-brown color. Examination of the surfaces after removal of corrosion products showed a non-uniform distribution of dissolution attack under these structures, as represented by Figure 15d for a 24 hour 10 ft/sec exposure; areas averaging about 100μm in diameter covered about 65 percent of the exposed surface; these broad areas are filled with more microscopic depressions averaging about 15μm in diameter. In general, more extensive areas of attack were observed for higher velocities, consistent with the higher corrosion currents recorded. It is considered that the effects of velocity observed here are essentially electrochemical, rather than mechanical. The observed variations in corrosion product morphology with velocity are consistent with the idea that higher velocities disfavor loosely adherent corrosion product masses, and favor a more compact product. It is not clear whether the mud-cracking of the compact film (as seen in Figure 15c) is a result of a cyclic cracking-spalling-redevelopment sequence under dynamic conditions, or is simply the result of drying. However, the former process seems likely, based on many observations.

The PCS anodic member of couples exposed statically did not exhibit any significant differences in corrosion product form, color, or distribution from static single-metal PCS samples (i.e. as Fig. 15a), but with some increase in the amount of product formed in a given time.

2. Dynamic Exposure of Couples

As for single-metal PCS specimens, coupled PCS exhibited dramatic changes in corrosion product morphology under dynamic conditions. Again, higher velocities promoted more compact and adherent structures, and more metal removal for a given time. Figures 16 and 17 presents typical structures observed at two velocities. There was little difference between the structures found on proximate and separated couples, and very little galvanic effect noticeable at the interface in proximate couples.

3. Cathodic Surfaces

The K-Monel and cupronickel samples showed no distinct surface morphological features (via SEM) after 24 hours for either single metal or cathodically coupled exposures. Under dynamic conditions, the only evidence of velocity on these cathodic metals, macroscopically, was a slight increase in metallic luster for the cupronickel, which was visibly brighter just after exposure at 10 ft/sec. This may be interpreted as an indication of an erosive scrubbing action or some change in character of the thin passive film. This subtle change may in fact have major significance, since the cathodic depolarization behavior is considered to be critical in these couples. However, a systematic study of changes on the cathode surfaces has not been conducted as yet, and discussion of this aspect will be reserved for a future report. The important role of the adherent passivating films on these materials has recently been reviewed by Syrett (1).

4. Discussion of Microscopic Effects

The morphological variations observed can be related to the RMS fluctuation in velocity, $\sqrt{\overline{V'^2}}$, over the surface (9% of 5 ft/sec, equivalent to 0.45 ft/sec, as compared with 6% of 10 ft/sec, equivalent to 0.60 ft/sec), as well as to the average free stream velocity, $\bar{V}$, the thickness of the hydrodynamic boundary layer, δ_h (and the related thickness of the diffusional sub-layer, δ_d), and perhaps the surface shear stress, τ_s. It is clear that as $\bar{V}$ increases, so does $\sqrt{\overline{V'^2}}$, and δ_h and δ_d decrease. Another factor is that of entrained bubbles in the electrolyte, which were created in the present situation by the wake action of the circulating foil, and would be generally caused by turbulence over upstream surfaces (as for hulls and pipes). With increased velocity, more air bubbles become entrained in the electrolyte; it is difficult to predict or quantify the amount in a given situation. However, it is clear that

if the air bubbles are of a critical diameter (the thickness of the hydrodynamic boundary layer, which decreases with $\bar{V}$,), bubbles striking the boundary layer are not deflected, and are subjected to differential forces that disrupt the boundary; this enables electrolyte to impinge more directly on the metal surface at the point of disruption, with possible erosive removal of metal or corrosion product structure. The higher the velocity, the more pronounced the above erosive component would be expected to be. In the present phase of work reported here (periods of up to 24 hours for velocities up to 3 m/sec) it is considered that the erosive (mechanical) component was generally negligible in comparison with the electrochemical (current) effects of velocity.

SUMMARY DISCUSSION

The electrochemical effects of dynamic conditions, which are considered to have dominated the changes in corrosion rate here, may be interpreted in terms of the effect of the flow field on the hydrodynamic and mass-transfer boundary layers. It is commonly known that as the average free stream velocity, $\bar{V}$, increases, turbulence, here represented by the RMS velocity fluctuation, $\sqrt{\overline{V'^2}}$, also increases, and there is a decrease in the thickness of the hydrodynamic boundary layer, which allows more rapid diffusion of ions to and from the surface reaction sites. Unfortunately, the exact mechanisms at work still remain somewhat vague. It is known, for example, that the electrochemical potential, E_{corr}, of many freely corroding copper alloys obtains a less noble potential and a higher corrosion current, i_{corr}, as $\bar{V}$ increases. Syrett (1) states that this effect is due to anodic depolarization, i.e., removal of anodically produced ions. By comparison, E_{corr} for PCS is known to become more noble as velocity increases in the range up to 4 m/sec (3), interpreted as the influence of more oxygen provision, with formation of a more compact form of corrosion product. This idea is confirmed by direct observations in the present studies. In terms of effects on the corrosion rate of PCS, increased velocity might be expected to increase the corrosion rate for short times, then decrease when the surface becomes covered, unless the compact film cracks, spalls, or otherwise allows passage of current. For the maximum times studied here (24 hours), no decrease was noticed; the corrosion current had typically either leveled off at a constant value or was still rising after this time.

It can be summarized that in a given dynamic situation, the changing electrochemical potentials of the free metals, the degree of cathodic and anodic polarization or depolarization, the thickness of the hydrodynamic boundary layer, the turbulence intensity, the geometry of the test system, entrained bubbles, the form and nature of corrosion products, and the time-dependence of some of these factors, combine to comprise an extremely complex experimental/environmental situation. It is no wonder that correlation of velocity effects data has historically been limited, and that interpretations of the effects quite superficial. In the present study, emphasis has been on accurate control and characterization of the fluid flow regime, together with direct and indirect monitoring of the corrosion processes. These approaches are considered to represent vitally important features of any fundamentally viable study of velocity effects on corrosion.

CONCLUSIONS

The following conclusions may be stated as a result of this study, specifically referring to 70-30 cupronickel/PCS and K-Monel/PCS couples in synthetic seawater.

1. Corrosion of galvanic couples under dynamic conditions is codependent on the basic electrochemical behavior of the metal components, and the hydrodynamic conditions imposed.
2. Galvanic current density (and corrosion rate) increases with increasing average free stream velocity, $\bar{V}$, for velocities up to 3 m/sec (10 ft/sec).
3. K-Monel cathodically polarizes more readily than 70-30 cupronickel, and cathodically depolarizes less under dynamic conditions, so that the corrosion rate of the associated anode will be less.
4. Increases in average free stream velocity result in an obvious change in single metal PCS corrosion product morphology, distribution, color, and rate of formation. At zero velocity the PCS corrosion product is quite loosely formed and deposited on the surface, with a bright orange color. As velocity increases, the corrosion product becomes more compact and darker in color.
5. For single metal PCS or at natural galvanic current densities (area ratio = 1.0), higher levels of the RMS velocity fluctuation of turbulent flow, $\sqrt{\overline{v'^2}}$, give rise to a more compact corrosion product formation. The corrosion product morphology changes from an irregular streaked topology at 1.5 m/sec

(5 ft/sec) to a very compact, form at 3 m/sec (10 ft/sec). This effect is noted regardless of couple type or configuration (proximate or separated).

6. There is evidence that an average freestream velocities around 3 m/sec, a cyclic film formation, cracking, spalling process occurs on PCS.
7. The amount of PCS corrosion product formed, and the degree of surface dissolution, are observed to increase with coupling, and to further increase with exposure under dynamic conditions, consistent with electrochemical measurements of the average current density.
8. The erosive (mechanical) component is insignificant relative to the electrochemical (current) effect of velocity for the exposures studied (24 hour periods at velocities up to 3 m/sec).

REFERENCES

1. B.C. Syrett, Corrosion, 32(1976) 242.
2. J.A. Davis, "Review of High Velocity Sea Water Corrosion T-7C-5 Task Group Report", Paper No. 101, Corrosion/78, San Francisco, California, 14-18 Mar 1977.
3. H.R. Copson, Corrosion 16(1960) 86t.
4. J.L. Basil, "The Corrosion of Metals as a Function of Sea-Water Velocity", 10 Jul 1964, Naval Engineering Laboratory Report 72/64.
5. J.L. Basil, "Corrosion of Materials in High Velocity Sea Water", U.S. Naval Engineering Experiment Station Report 910160A, Dec. 1960.
6. G.J. Danek, Jr., Naval Engineers Journal, p. 763, Oct 1966.
7. "Cathodic Protection of Surface Effect Ships at High Speeds", Bell Aerosystems Company, Ocean City Research Corporation Final Report 1-35551, Sept 1975.
8. J.A. Davis and G.A. Gehring, Jr., Materials Performance, 14(1975) 32.
9. J.A. Davis and G.A. Gehring, Jr., Paper No. 123, Corrosion/75, Toronto, Canada, 14-18 Apr 1975.
10. J.A. Davis and G.A. Gehring, Jr., Paper No. 75, Corrosion/76, Houston, Texas, 22-26 Mar 1976.
11. K.D. Efird, Paper presented at the Corrosion Research Conference of Corrosion/76, Houston, Texas, 22-26 Mar 1976.
12. J.A. Davis, A.A. Watts, and G.A. Gehring, Jr., Paper presented at the Electrochemical Society 150th Annual Conference, Las Vegas, Nevada, 18-22 Oct 1976.

ACKNOWLEDGEMENT

This work was supported by the Office of Naval Research, Metallurgy Program Office, through Contract NR 036-120, and by the Naval Postgraduate School Foundation Research Program.

TABLE I

	OUTBOARD		CENTERLINE		INBOARD	
V	5 (ft/sec)	10	5 (ft/sec)	10	5 (ft/sec)	10
$\frac{\sqrt{\overline{v'^2}}}{\bar{V}}$	0.093	0.065	0.094	0.065	0.097	0.068

FIGURE CAPTIONS

Figure 1: Overall view of dynamic exposure apparatus, showing tank, foil assembly and control and recording equipment.

Figure 2: Specimen-carrying foil deployed on vertical strut from horizontal rotating arm.

Figure 3: Close-up view of specimen-carrying foil, showing locations of specimens and electrical contacts. The strut is at the back of the foil as it moves through the electrolyte.

Figure 4: Detail of specimen-carrying foil.

Figure 5: Detail of specimen cavity in topside of foil.

Figure 6: Specimen mounts used to hold single metals and couples. From left-to-right, top-to-bottom: torque wrench used to apply reproducible contact stress between mounted proximate couples, unmounted specimen coupons, proximately-located coupons in special mounting ring prior to moulding, finished proximate couple mount, finished single metal mount, finished single metal mount for separated couple.

Figure 7: Foil assembly with hot-film probe mounted over center specimen position.

Figure 8: Schematic showing construction of a hot-film probe.

Figure 9: Plots of $\sqrt{V}$ vs. e^2 for each specimen position on the foil, showing extrapolated values of V_o.

Table I: Experimentally determined values of turbulence intensity over the foil surface (5 ft/sec = 1.5 m/sec, 10 ft/sec = 3.0 m/sec).

Figure 10: Polarization curves for 70/30 cupronickel and PCS under static conditions.

Figure 11: Polarization curves for K-Monel and PCS under static conditions.

Figure 12: Galvanic current density i_{couple}, vs. time for 70-30 cupronickel/PCS couples at various velocities. (5 ft/sec = 1.5 m/sec, 10 ft/sec = 3.0 m/sec).

Figure 13: Galvanic current density, i_{couple}, vs. time, for K-Monel/PCS couples at various velocities (5 ft/sec = 1.5 m/sec, 10 ft/sec = 3.0 m/sec).

Figure 14: Average corrosion rate (in 24 hour period) as a function of velocity for 70-30 cupronickel/PSC and k-Monel/PCS couples.

Figure 15: SEM photographs of single metal PCS specimen surfaces after various exposures: (a) 24 hours static, 610x, (b) 24 hours at 1.5 m/sec, 115x, (c) 24 hours at 3 m/sec, 130x, (d) 24 hours at 3 m/sec, after ultrasonic cleaning, 235x.

Figure 16: SEM photographs of surface of PCS in 70-30 cupronickel/PCS proximate couples after various exposures: (a) 24 hrs., 1.5 m/sec, 20x, (b) 24 hrs., 1.5 m/sec, cleaned 600x, (c) 24 hrs., 3.0 m/sec, 250x, (d) 24 hrs., 3.0 m/sec, cleaned, 235x; note interface with cupronickel at left.

Figure 17: SEM photographs of surface of PCS in 70-30 cupronickel/PCS separated couples after various exposures: (a) 24 hrs., 1.5 m/sec, 600x, (b) 24 hrs., 1.5 m/sec, cleaned, 610x, (c) 24 hrs., 3.0 m/sec, 550x, (d) 24 hrs., 3.0 m/sec, cleaned, 225x.

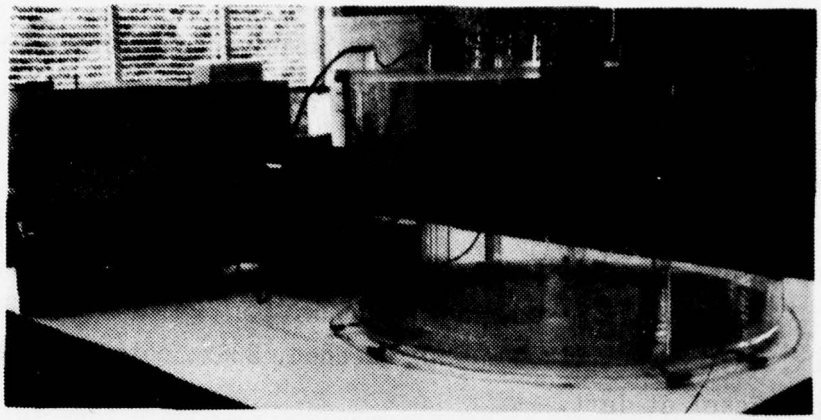

Figure 1: Overall view of dynamic exposure apparatus, showing tank, foil assembly, and control and recording equipment.

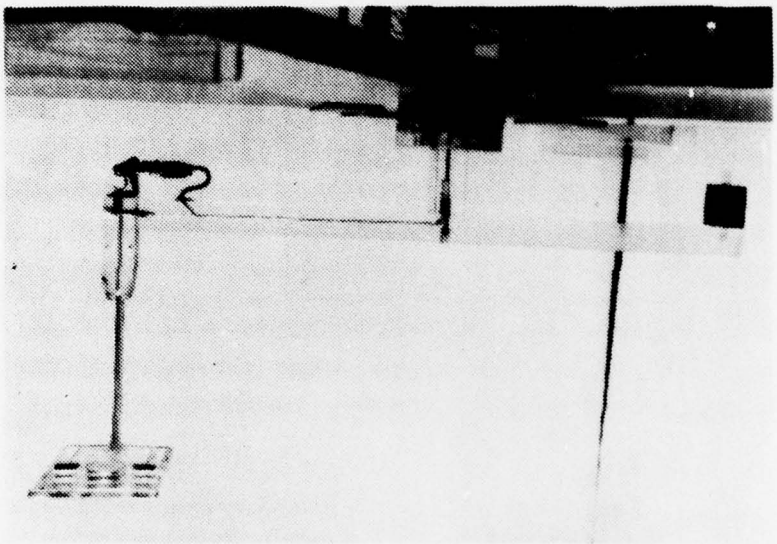

Figure 2: Specimen-carrying foil deployed on vertical strut from horizontal rotating arm.

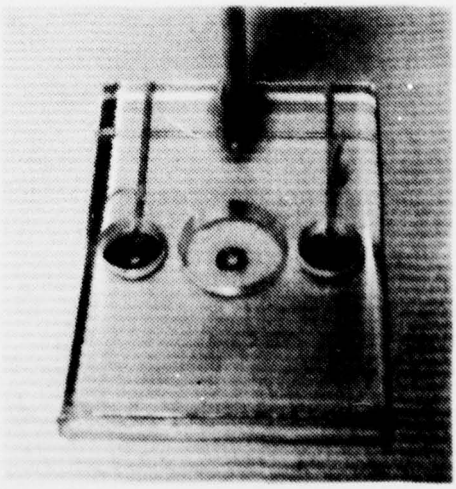

Figure 3: Close-up view of specimen-carrying foil, showing locations of specimens and electrical contacts. The strut is at the back of the foil as it moves through the electrolyte.

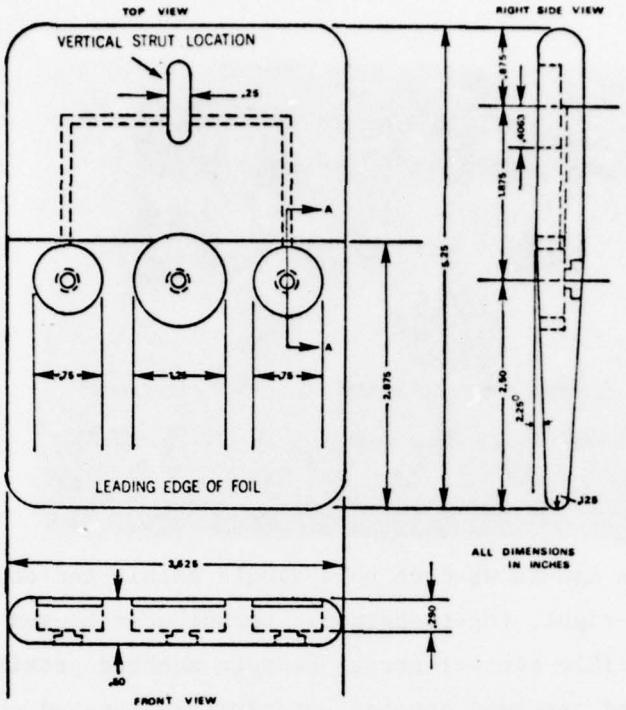

Figure 4: Detail of specimen-carrying foil.

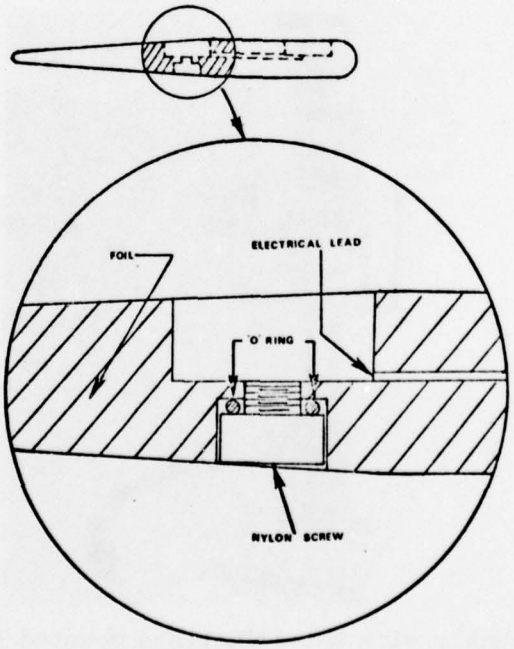

Figure 5: Detail of specimen cavity in topside of foil.

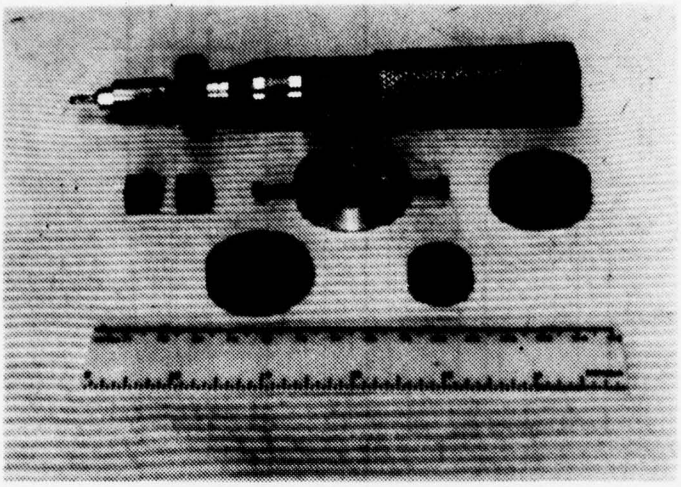

Figure 6: Specimen mounts used to hold single metals and couples. From left-to-right, top-to-bottom: torque wrench used to apply reproducible contact stress between mounted proximate couples, unmounted specimen coupons, proximately-located coupons in special mounting ring prior to moulding, finished proximate couple mount, finished single metal mount, finished single metal mount for separated couple.

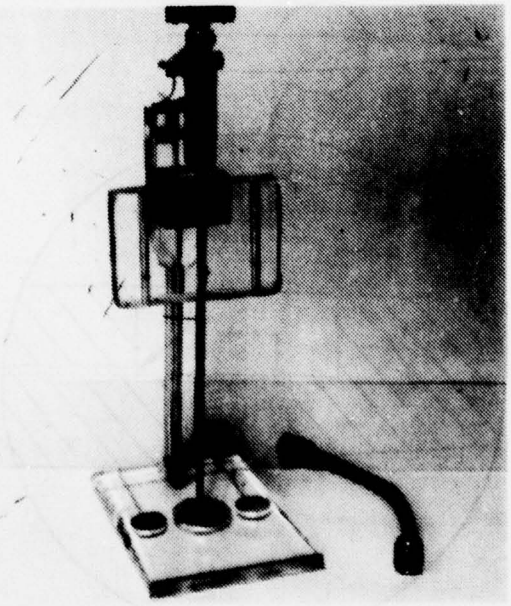

Figure 7: Foil assembly with hot-film probe mounted over center specimen position.

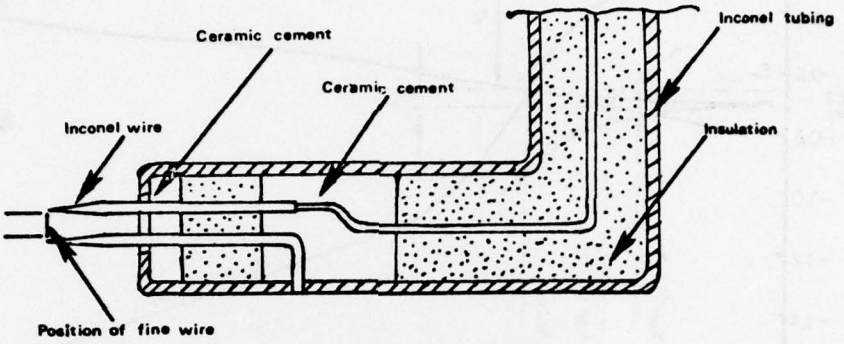

Figure 8: Schematic showing construction of a hot-film probe.

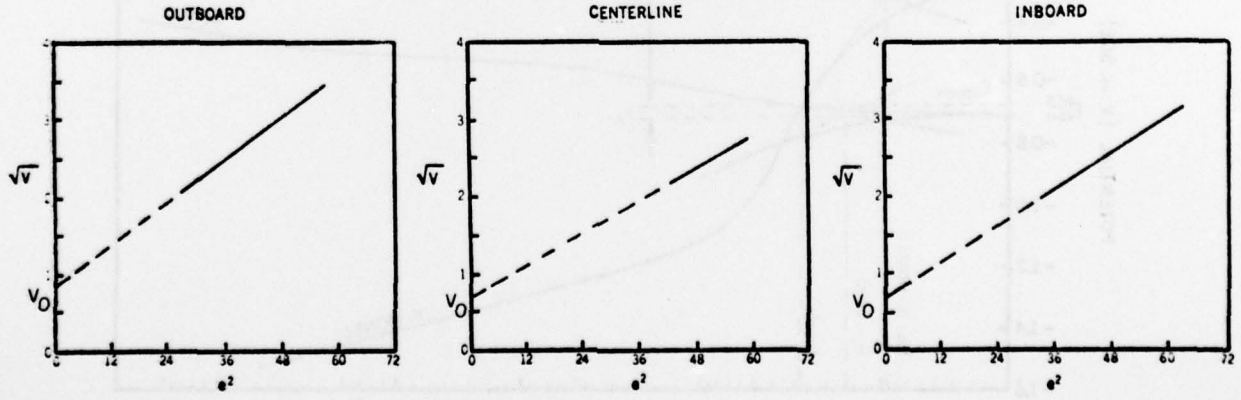

Figure 9: Plots of $\sqrt{V}$ vs. e^2 for each specimen position on the foil, showing extrapolated values of V_o.

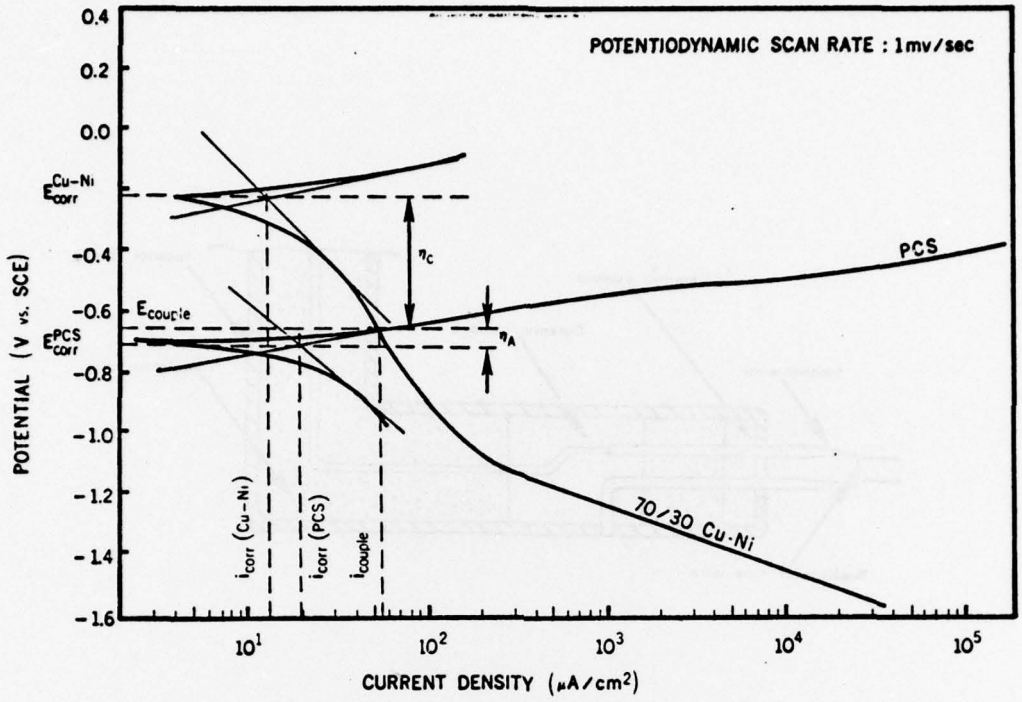

Figure 10: Polarization curves for 70/30 cupronickel and PCS under static conditions.

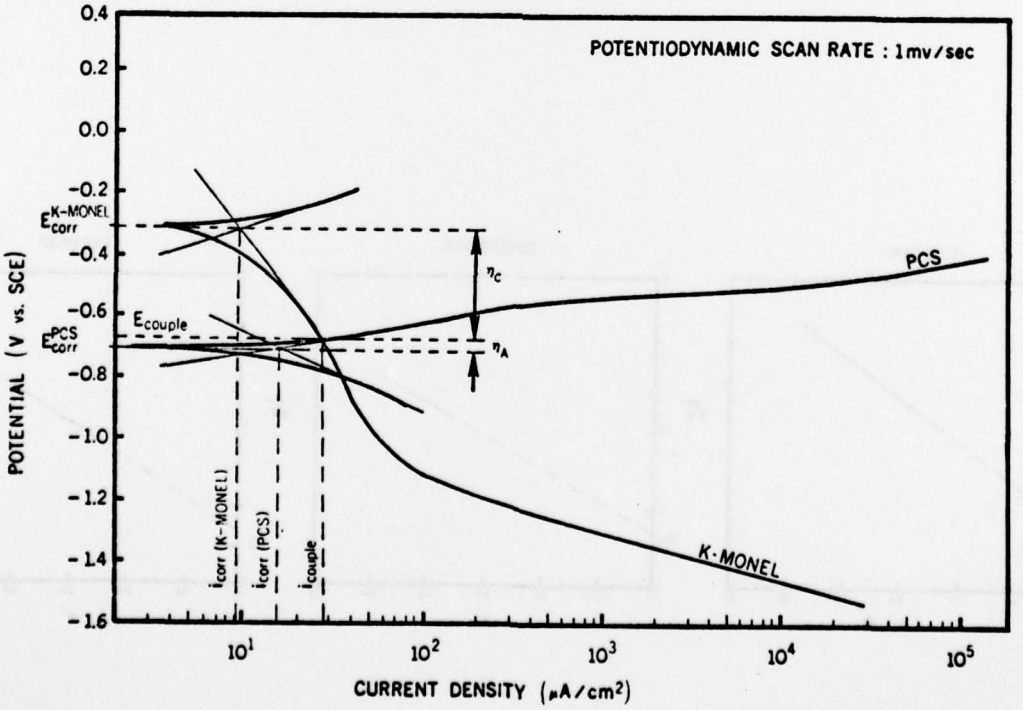

Figure 11: Polarization curves for K-Monel and PCS under static conditions.

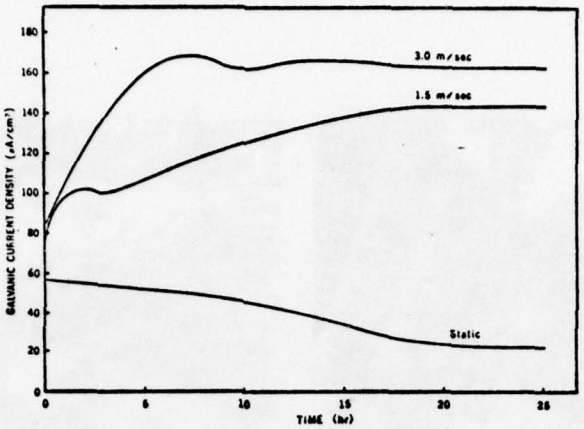

Figure 12: Galvanic current density, i_{couple}, vs. time for 70-30 cupronickel/PCS couples at various velocities. (5 ft/sec = 1.5 m/sec, 10 ft/sec = 3.0 m/sec).

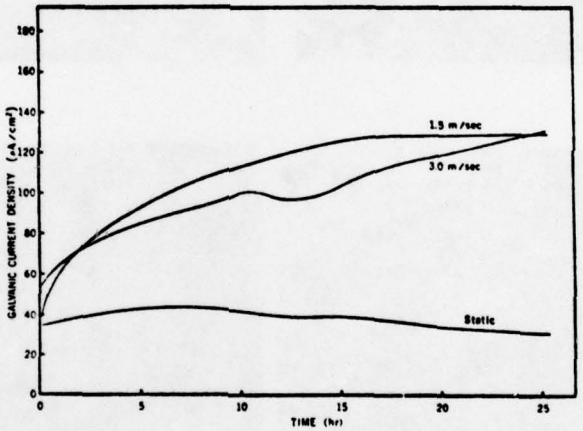

Figure 13: Galvanic current density, i_{couple}, vs. time, for K-Monel/PCS couples at various velocities (5 ft/sec = 1.5 m/sec, 10 ft/sec = 3.0 m/sec).

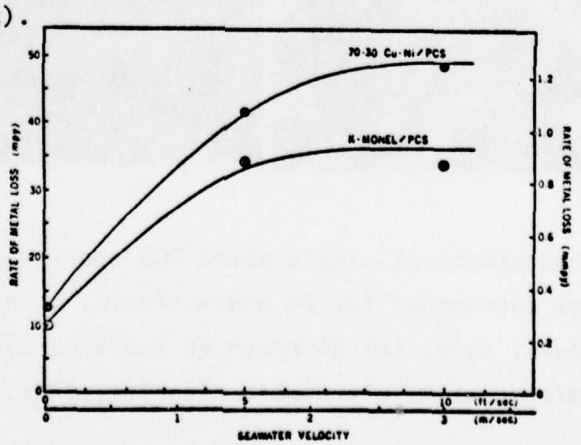

Figure 14: Average corrosion rate (in 24 hour period) as a function of velocity for 70-30 cupronickel/PCS and K-Monel/PCS couples.

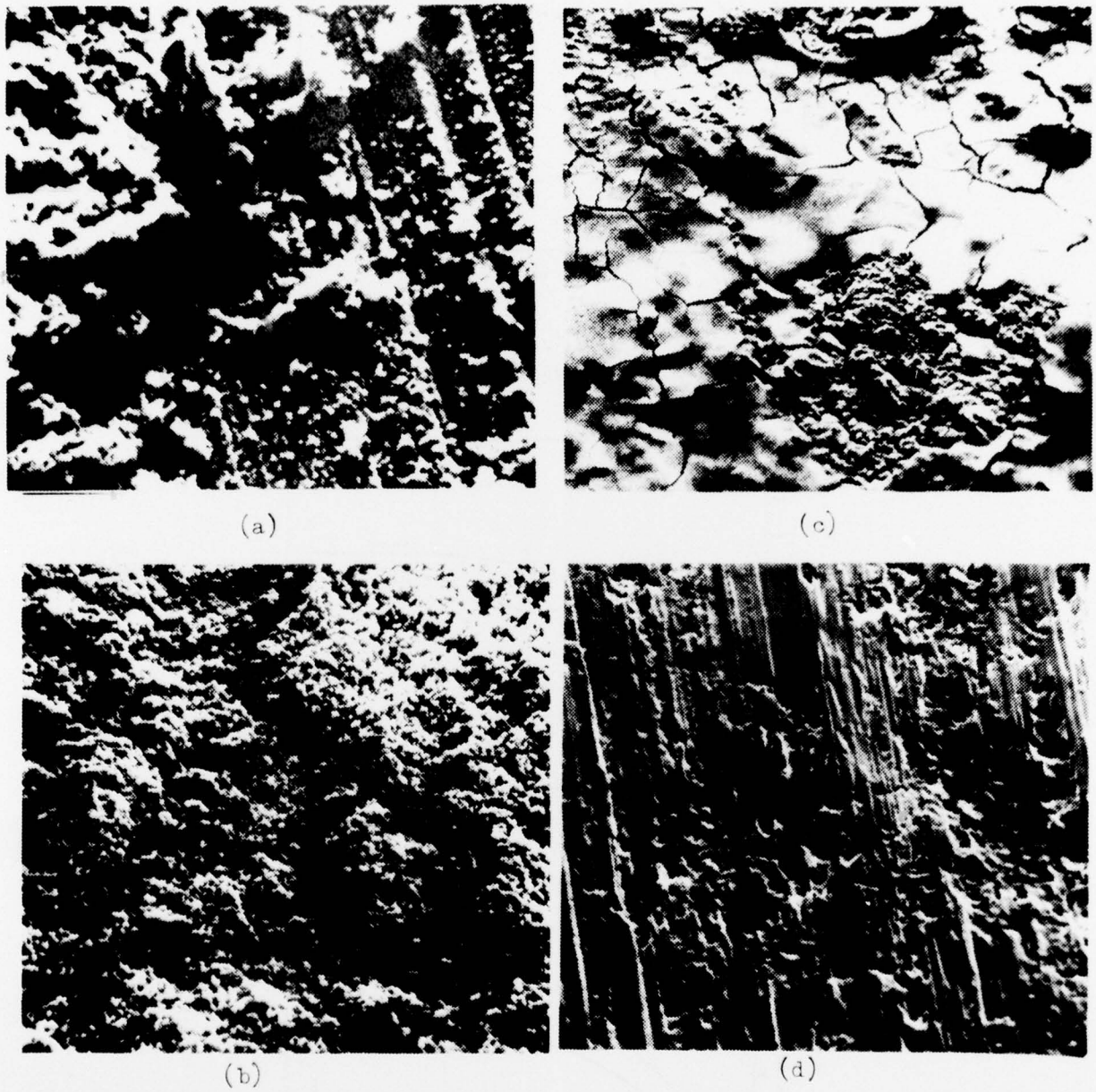

Figure 15: SEM photographs of single metal PCS specimen surfaces after various exposures: (a) 24 hours static, 610x, (b) 24 hours at 1.5 m/sec, 115x, (c) 24 hours at 3 m/sec, 130x, (d) 24 hours at 3 m/sec, after ultrasonic cleaning, 235x.

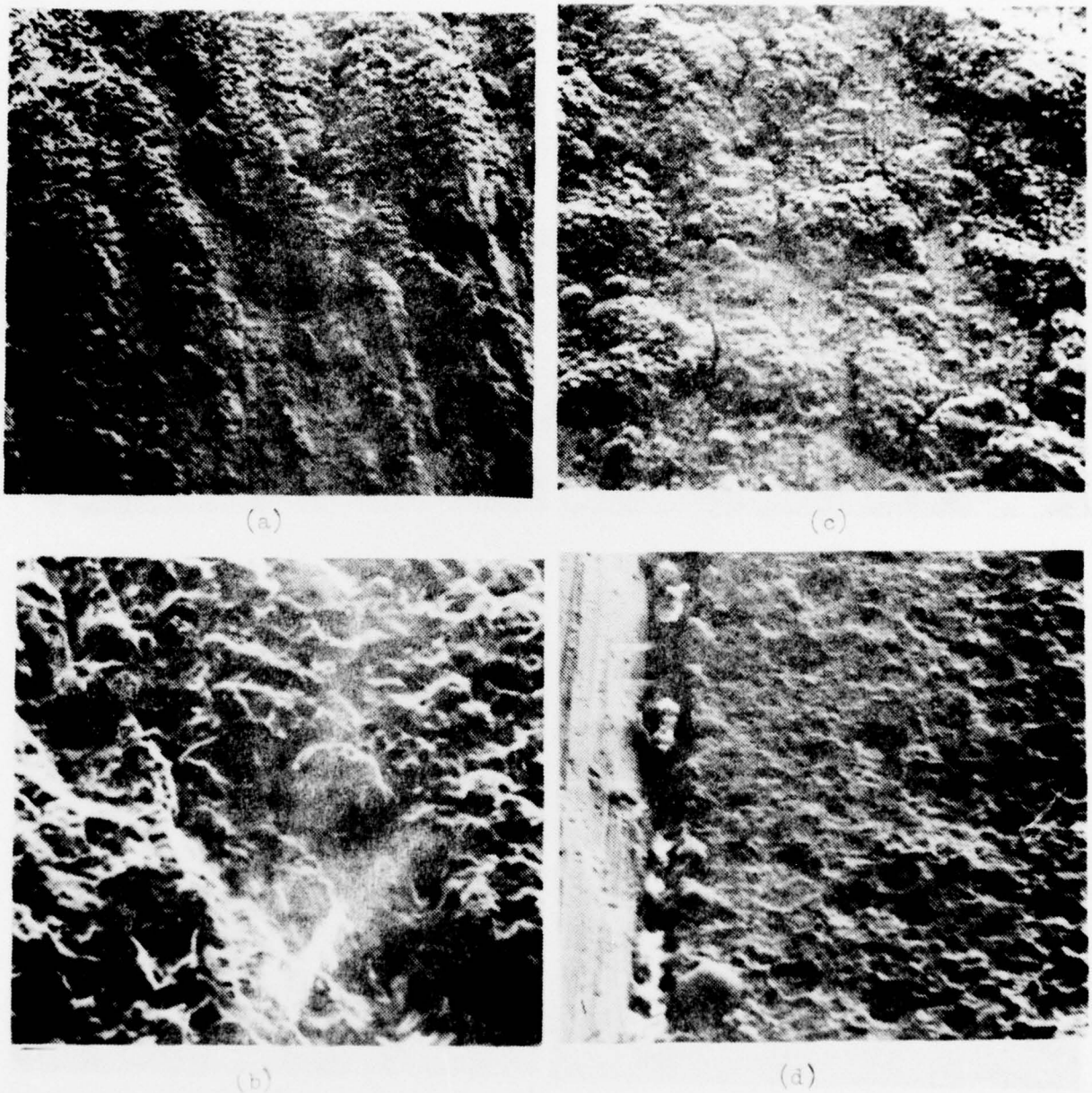

Figure 16: SEM photographs of surface of PCS in 70-30 cupronickel/PCS proximate couples after various exposures: (a) 24 hrs., 1.5 m/sec, 20x, (b) 24 hrs., 1.5 m/sec, cleaned 600x, (c) 24 hrs., 3.0 m/sec, 250x, (d) 24 hrs., 3.0 m/sec, cleaned, 235x; note interface with cupronickel at left.

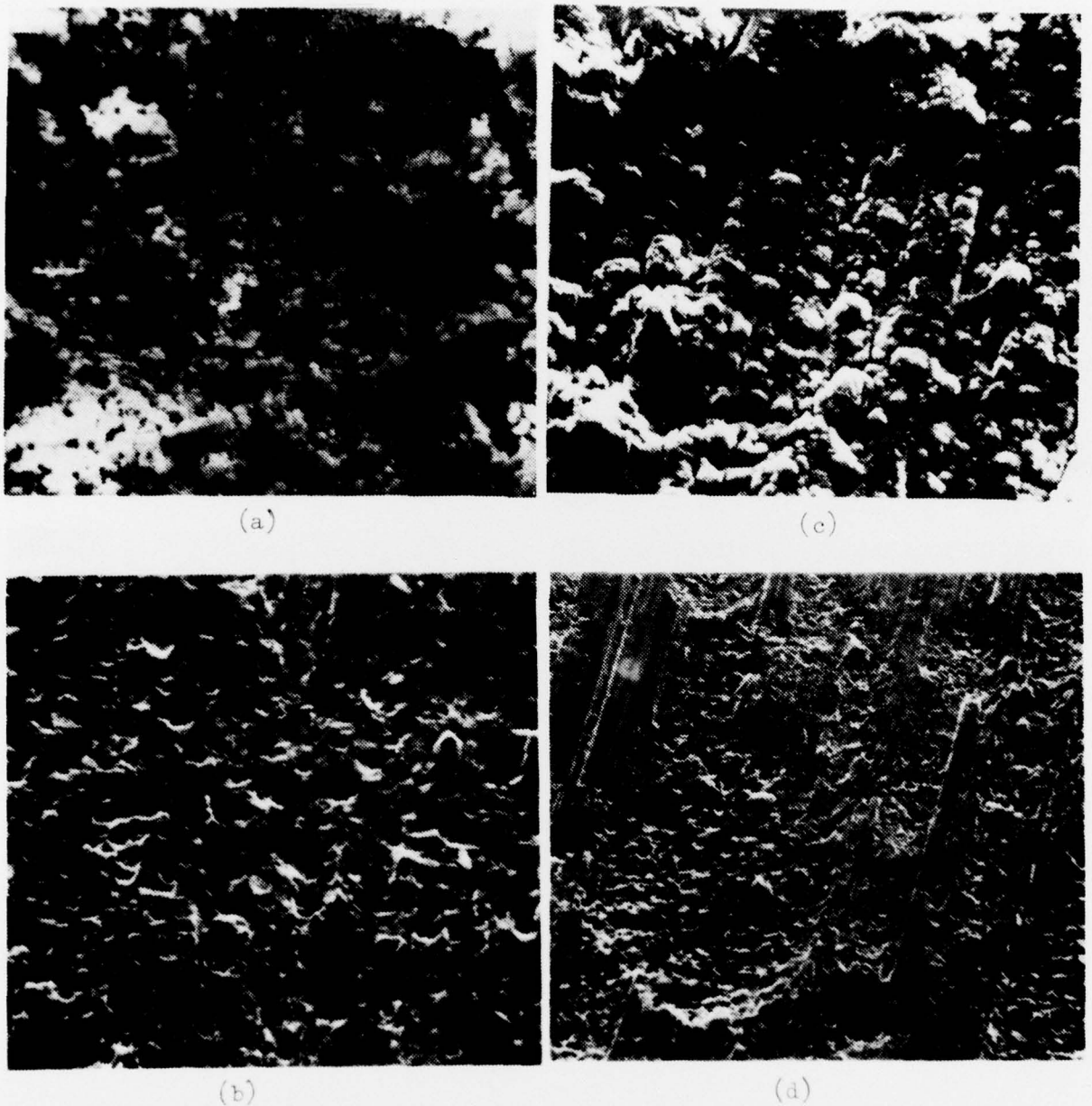

Figure 17: SEM photographs of surface of PCS in 70-30 cupronickel/PCS separated couples after various exposures: (a) 24 hrs., 1.5 m/sec, 600x, (b) 24 hrs., 1.5 m/sec, cleaned, 610x, (c) 24 hrs., 3.0 m/sec, 550x, (d) 24 hrs., 3.0 m/sec, cleaned, 225x.